Available online at www.sciencedirect.com
ScienceDirect
Trans. Nonferrous Met. Soc. China 32(2022) 3973−3984
Transactions of Nonferrous Metals Society of China
www.tnmsc.cn

Diffusion bonding behaviour of β−γ TiAl alloys containing high niobium with Ti interlayer by spark plasma sintering

Qiang GAO, Lai-qi ZHANG, Yi QIAO, Jun-pin LIN

State Key Laboratory for Advanced Metals and Materials,
University of Science and Technology Beijing, Beijing 100083, China

Received 29 September 2021; accepted 15 August 2022

Abstract: High niobium β−γ TiAl alloy (HNBG) was diffusion bonded using spark plasma sintering with pure Ti as interlayer. The joint microstructural evolution, growth kinetics and mechanical properties were investigated. The joint included three diffusion zones. The β/$B2$ phase formed in the Zone I, α_2 phase in the Zone II, and β-Ti and α-Ti phases in the Zone III. The thickness of β/$B2$ phase, the average grain size of α_2 phase and the amount of β-Ti phase increased with the increase of bonding temperature or bonding time. The growth activation energies of β/$B2$ and α_2 phases were 582 and 253 kJ/mol, respectively. The joint acquired at 1000 °C, 10 min and 10 MPa showed the maximum shear strength of 308 MPa. Fracture mainly occurred along the interfaces between Zone I and HNBG alloy, and between Zone I and Zone II. Fracture mechanism of the joint was characterized by brittleness rupture along the phase boundary.

Key words: high niobium β−γ TiAl alloy; diffusion bonding; spark plasma sintering; interlayer; microstructure evolution; mechanical properties

1 Introduction

At present, β−γ TiAl alloys have attracted much concern as a lightweight high temperature structure material [1]. Compared with traditional TiAl alloys, β−γ TiAl alloys have a better hot processing capacity owing to containing bcc β phase with enough slip systems by utilizing β-stabilizing alloying elements, such as Nb, Mo, Cr, V and Mn [2]. Up to now, β−γ TiAl alloys with different compositions have been developed [3−5], which are featured by uniform microstructure, weak texture and small degree of segregation. What's more, high niobium β−γ TiAl alloy (HNBG alloy) has been forged with no can by our group [6]. Consequently, HNBG alloy is superior in manufacturing some complex components using hot working method, for instance, the isothermal forging [3]. However, some complex components, such as the parts that need to be assembled as hollow engine blade, can almost only be fabricated by the joining technology [7]. Therefore, the research for the bonding of HNBG alloys is necessary to broaden the engineering application fields.

Diffusion bonding process was carried out under the melting point of the materials to be joined and by applying pressure at the same time [8]. This technique has several advantages, such as avoiding the cracking encountered during fusion welding, producing joints with hardly a macroscopic deformation and scarcely generating metallurgical deterioration [8,9]. Therefore, the diffusion bonding has been regarded as the effective joining method to bond TiAl alloys because of its limited ductility and toughness along with the sensitivity to hot cracking [10]. YAN and WALLACH [11] successfully joined as-cast TiAl(Ti−48Al(at.%))

Corresponding author: Lai-qi ZHANG, Tel: +86-13552059009, E-mail: zhanglq@ustb.edu.cn
DOI: 10.1016/S1003-6326(22)66071-0

alloy and good bend properties were achieved in the condition of room temperature and 600 °C. MASAHASHI et al [12] compared the joint shear strength of TiAl alloy at different microstructure states, including γ/β dual phase fine grain microstructure and γ/α_2 coarse grain microstructure, and the result showed that the joint strength of the former was relatively high. In order to reduce bonding temperature or time, the utilization of interlayer is the common choice. DUARTE et al [13] used alternating Ti/Al nanolayers to bond γ-TiAl alloy, the result showed that sound joint was obtained at 900 °C, 50 MPa and 1 h, while higher temperature and longer time (1000 °C, 20 MPa, 5 h) were needed to achieve sound bond without using interlayer [7]. Although nanolayers are efficient in joining TiAl alloy, the process is relatively complicated. Single interlayer, such as pure Ti foil used in the joining is contrarily proved to be an effective and simple process [14−16]. However, the diffusion bonding was performed using hot pressing method which needed longer bonding time even if the interlayer was used. Spark plasma sintering (SPS) is generally applied for powder sintering through pulse current generating joule heat, and it features a fast heating rate and short sintering time, thus low energy consumption [17]. On the basis of this rapid heating method, it can also be used to conduct the diffusion bonding. Compared with hot pressing diffusion bonding, the diffusion bonding by SPS can accelerate the atom diffusion rate through electrical migration effect, and this can enhance the performance of joints [18,19]. ZHANG et al [20] used SPS to bond Ti−46Al−2Cr (at.%) alloy and Ti_2AlNb alloy with Ti interlayer, the result displayed that the sound joint can be obtained at 950 °C, 8 MPa and 60 min, and the tensile strength of the joint was 454 MPa. However, the maximum tensile strength of the joint was 281 MPa when the TiAl alloy was bonded to Ti_2AlNb alloy with Ti interlayer using hot pressing method [21]. At present, there has been no report on the diffusion bonding of β−γ TiAl alloy with similar or dissimilar materials using interlayers by SPS. Due to the existence of relatively large amount of β phase stable elements, the joint microstructure of β−γ TiAl alloy unavoidably will be distinct from that of conventional TiAl alloys when diffusion bonding is conducted with interlayer. Consequently, the investigation on relationship between the joint microstructure and properties is also necessary. In this work, the HNBG alloy was bonded with Ti foil interlayer by SPS. The effects of bonding temperature and time on the joint microstructure were investigated. The relationship between the joint microstructural evolution and the mechanical properties was investigated.

2 Experimental

The HNBG alloy was used in annealing state. The microstructure was displayed in the previous study [19]. The size of HNBG alloy sample machined by electrical-discharge machining was also the same with previous study [19]. The final mating surfaces were ground with 1200# SiC paper. Pure Ti foil with 100 μm was ground to (30±10) μm using 1200# SiC paper. The optical microstructure and XRD pattern of Ti foil are shown in Fig. 1, which is featured by equiaxed grains of α-Ti occupied by some twin structures. All specimens were cleaned by acetone in the ultrasonic bath for 20 min before perfoming the diffusion bonding. The Ti foil was interposed between two HNBG alloy samples as a sandwich which was wrapped by adhesive tape. And then the sandwich

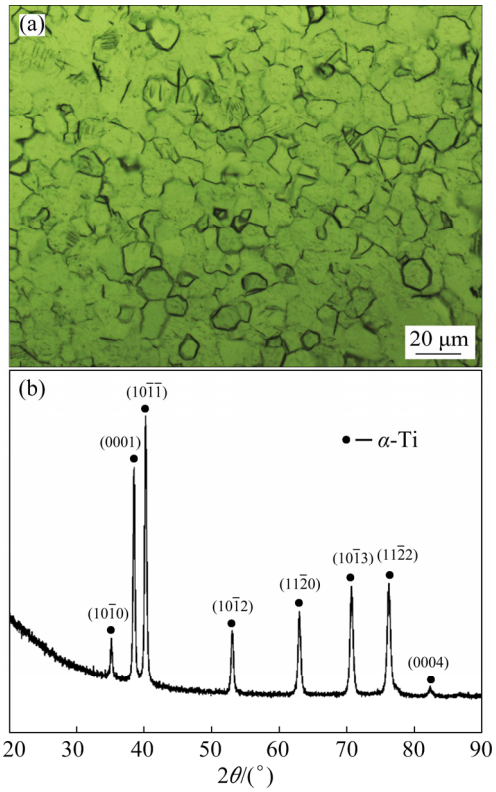

Fig. 1 Optical microstructure (a) and XRD pattern (b) of pure Ti foil

structure was put into a graphite die with graphite punches being 50 mm in diameter for diffusion bonding. The bonding temperature varied from 900 to 1050 °C and bonding time from 5 to 20 min at the bonding pressure of 10 MPa. The heating rate was set at 100 °C/min and the joining process was conducted at around 5×10^{-2} Pa.

Phase constituents analysis was done by X-ray diffraction (XRD, DMAX-RB, Rigaku) with Cu K_α radiation. The joint microstructures were investigated using a scanning electron microscope (SEM, SUPRA−55, Zeiss) equipped with an energy dispersive spectroscopy (EDS) and a HKL fast acquisition EBSD system. The samples for EBSD were prepared by polishing with diamond down to 0.5 μm firstly, and then by polishing with 0.05 μm colloidal silica suspension for 1 h. The BSE images were transformed to binary images using photoshop for statistics of phase content. Five images were counted for each parameter. Shear samples with a shear area of 4 mm × 4 mm (bonding area) were used. Vicker's hardness measurement of joint was performed under a load of 25 g and with a dwell time of 15 s. The shear properties were tested at room temperature with a loading speed of 0.5 mm/min and three parallel samples were adopted. The schematic diagram of shear tool is displayed in Fig. 2.

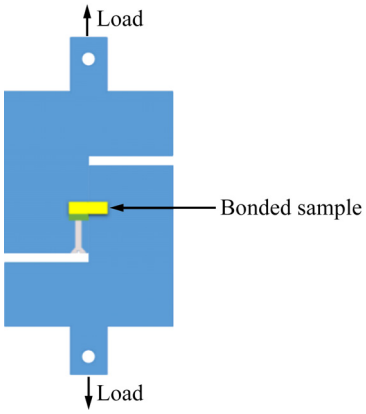

Fig. 2 Schematic diagram of shear sample and shear tool

3 Result and discussion

3.1 Typical joint microstructure of HNBG alloy bonding with Ti foil

Figure 3 shows the typical interfacial microstructure of HNBG alloy joint bonding with Ti foil at 950 °C, 10 min and 10 MPa. According to the phase morphology and contrast in Fig. 3(a), the joint is divided into three diffusion zones. The diffusion Zone I next to HNBG alloy was composed of light gray phase, the interface between Zone I and HNBG alloy was relatively straight, while that between Zone 1 and Zone II was relatively curved. The diffusion Zone II consisted of small equiaxed grains, as can be observed from Fig. 3(c). The diffusion Zone III contained large amount of dark grey lamellar phase, slight amount of light grey lamellar and dark phases. To identify the phases in each diffusion zone, the element quantitative analysis from Spots 1 to 5 by EDS was performed and the results are listed in Table 1. For some phases cannot be determined only using EDS, the EBSD observations were carried out at the interface. According to EDS result of Spot 1, the light gray phase in Zone I can be considered as β/*B*2 phase, which can also be confirmed by EBSD result in Fig. 3(c). In Zone II, combining EDS result (labeled as 2) with phase distribution map in Fig. 3(c), the small equiaxed grains should be composed of α_2-Ti_3Al phase. In Zone III, according to EBSD result in Fig. 3(c), the dark grey lamellar phase at Spot 3 should be α-Ti phase while light grey lamellar phase at Spot 4 cannot be sheared by EBSD because of small size. The composition of dark phase at Spot 5 is close to pure Ti. It is indicated that the diffusion distance of Al, Nb, Cr and Mn atoms is short in the Ti interlayer due to low bonding temperature. According to Ti−Al−Nb ternary phase diagram in Fig. 4 [22], it should be α-Ti phase. In order to determine the phase at Spot 4, the bonded sample was step by step ground perpendicularly to the diffusion direction (as marked in Fig. 3(a)) until the Zone III completely appeared, then, XRD was conducted on this grinding surface. In Fig. 3(d), the XRD pattern shows that among the diffraction peaks, the main strong peaks are related to α-Ti besides some relative weak peaks of β-Ti. In addition, the content of light grey lamellar phase is obviously smaller than the total content of dark grey lamellar and dark phases in Zone III. Therefore, the light grey lamellar phase at Spot 4 should be β-Ti phase. In addition, it is obvious that the relative intensity of the (0001) peak of α-Ti in Fig. 3(d) is stronger than that in Fig. 1(b), indicating that part α-Ti phase showed (0001) preferred orientation after the diffusion bonding different from the random orientation of α-Ti phase in original pure Ti foil.

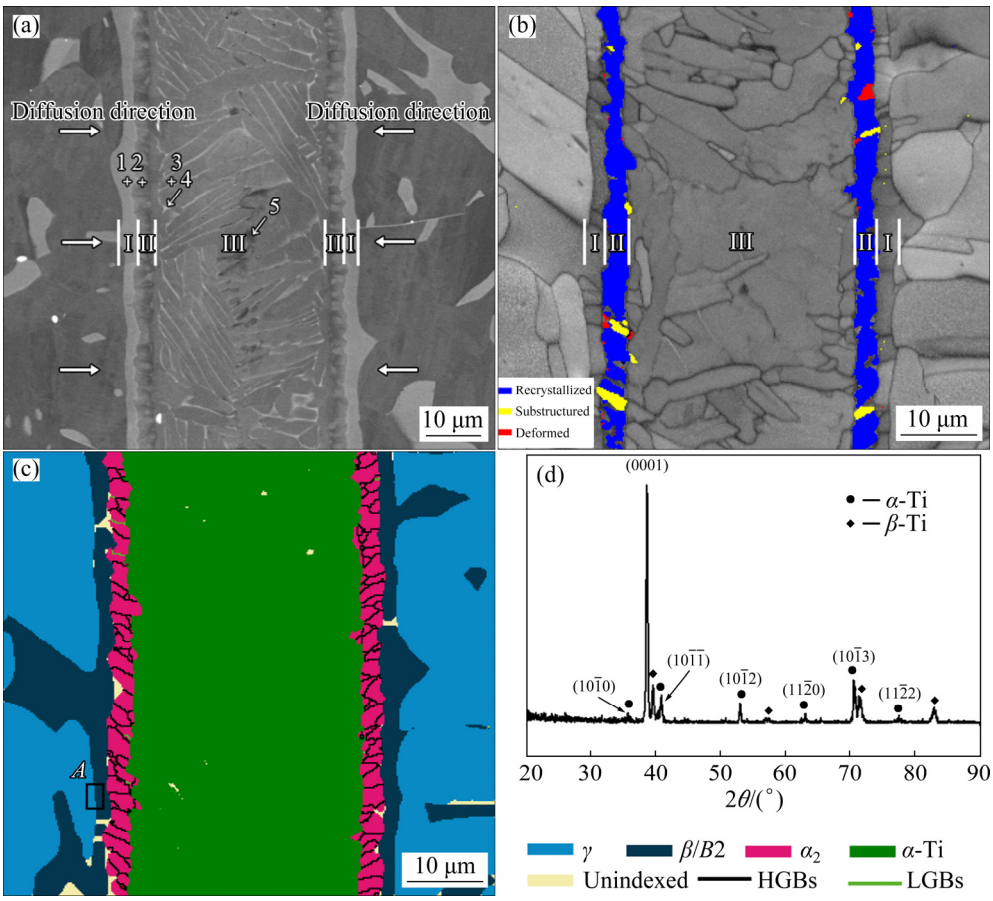

Fig. 3 Microstructure and phase analysis of HNBG alloy joints bonded with Ti foil at 950 °C, 10 min and 10 MPa: (a) BSE image; (b) Band contrast map overlapped with recrystallization map of Zone II; (c) Phase distribution map overlapped with grain boundaries of Zone II; (d) XRD pattern of Zone III

Table 1 EDS analysis at locations marked in Fig. 3(a) (at.%)

Spot No.	Ti	Al	Nb	Mn	Cr	Possible phase
1	53.55	35.74	9.13	0.77	0.81	*B*2
2	64.34	29.21	6.15	0.30	–	α_2
3	92.53	6.78	0.68	–	–	*α*-Ti
4	91.81	6.57	1.08	0.55		*β*-Ti
5	94.61	4.95	0.4	–	–	*α*-Ti

3.2 Effect of bonding parameters on joint microstructure of HNBG alloy bonding with Ti foil

Figure 5 shows the effects of bonding parameters on the joint microstructure of HNBG alloy joints bonding with Ti interlayer at 10 MPa. Figures 5(a, c, e) display the joint microstructure at different bonding temperatures. In Zone I, the width of diffusion layer increased with the increase of the bonding temperature, and Zone I was also close to lower convex parabolic growth as a function of temperature. The interdiffusion of Al atoms from the HNBG alloy and Ti atoms from the interlayer made the *γ* phase poor Al and rich Ti, resulting in transformation of *γ* to *β*/*B*2 phase in the joint, which can also be confirmed in Fig. 6. The {111} crystal plane of *γ* phase is parallel to the {110} crystal plane of the *β*/*B*2 phase together with ⟨110⟩ crystal direction of *γ* phase parallel to ⟨111⟩ crystal direction of the *β*/*B*2 phase. The existing orientation relationship of *γ* phase and *β*/*B*2 phase indicates the occurrence of transformation of *γ* to *β*/*B*2 phase. The relationship between width of diffusion layer and the diffusion time can be described by upper convex parabola function as follows [23]:

$$w^2=kt \tag{1}$$

$$k=k_0\exp[-Q/(RT)] \tag{2}$$

where w is the width of diffusion Zone I, k is the growth rate ($m^2\cdot s^{-1}$), t is the diffusion time (s), k_0 is the growing rate constants ($m^2\cdot s^{-1}$), R is the gas constant (8.31 $J\cdot mol^{-1}\cdot K^{-1}$), T is the thermodynamic

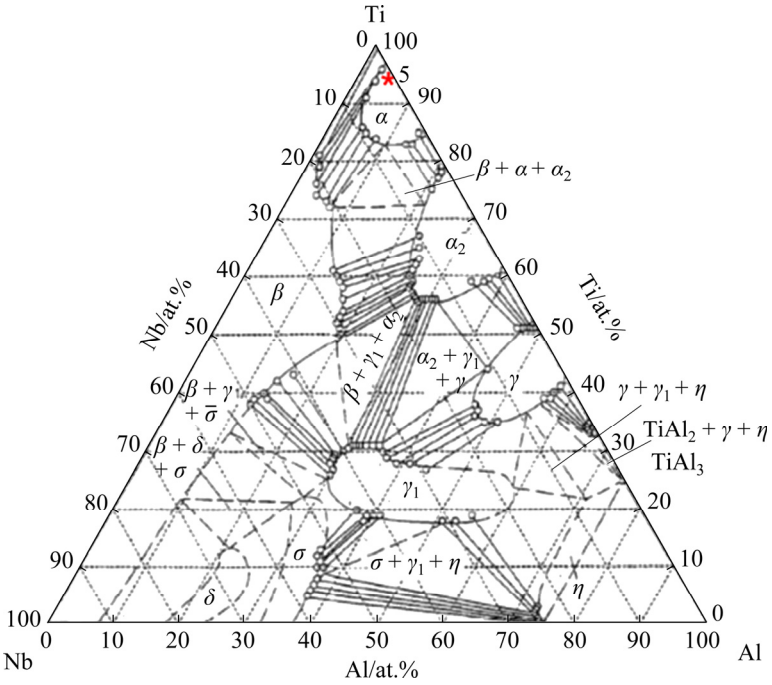

Fig. 4 Ti−Al−Nb ternary phase diagram at 1000 °C [22]

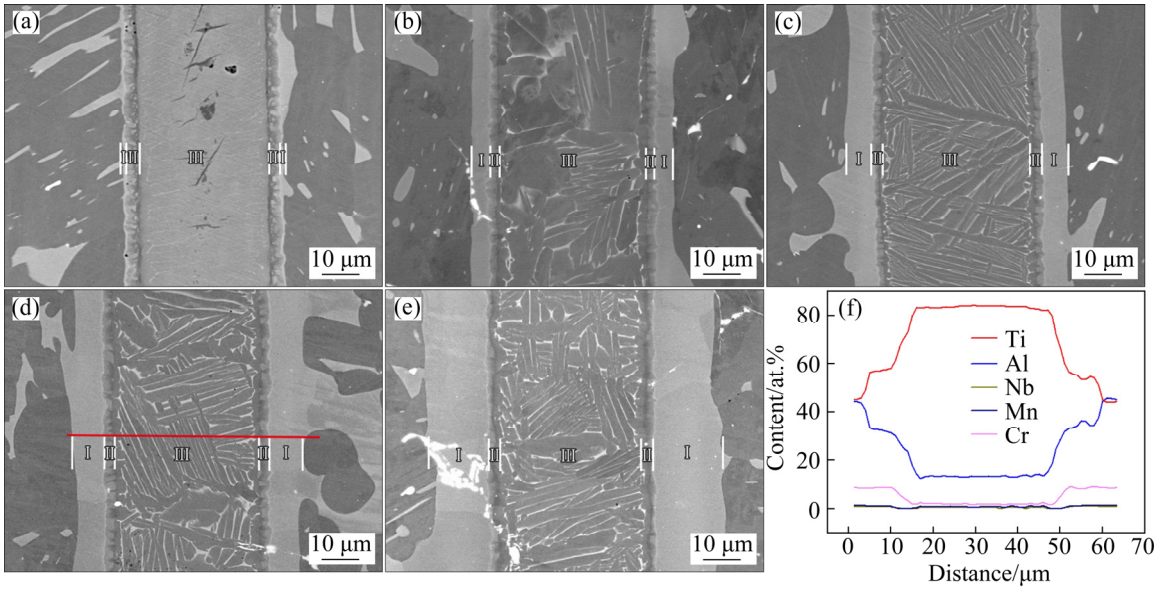

Fig. 5 BSE microstructures of HNBG alloy joints bonded with Ti foil at 10 MPa: (a) 900 °C, 10 min; (b) 1000 °C, 5 min; (c) 1000 °C, 10 min; (d) 1000 °C, 20 min; (e) 1050 °C, 10 min; (f) EDS linear scanning result of HNBG alloy joint bonded at 1000 °C and 20 min

temperature (K), and Q is the activation energy for growth. By plugging Eq. (1) into Eq. (2), and the logarithm of both sides, the relationship between width of Zone I and temperature can be expressed as

$$\ln(w^2/t)=2\ln k_0-Q/(RT) \quad (3)$$

Figure 7(c) displays the fitting result on the growth behavior of diffusion layer in Zone I. The growth activation energy of $\beta/B2$ phase is fitted to be 582 kJ/mol. As for Zone II, there existed high angle grain boundaries (HAGBs) mostly and low angle grain boundaries (LAGBs) can hardly be detected in α_2 phase, as can be seen from Fig. 3(c), which means that dynamic recrystallization(DRX) occurred in this zone. The occurrence of DRX in Zone II can also be confirmed by recrystallization map of Zone II in Fig. 3(b). In addition, the average

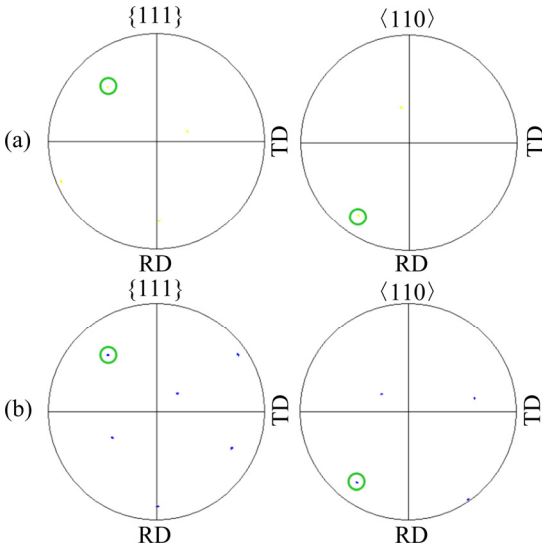

Fig. 6 Pole figures of γ (a) and β/*B*2 (b) phases of Area *A* in Fig. 3(c)

grain size is calculated from Fig. 8, and the corresponding result is displayed in Fig. 9(a) and the average grain size increased with the bonding temperature. When the bonding temperature increased to 1050 °C, the average grain size reached 3.4 μm. The relationship between grain size of α_2 phase and the bonding time can be described by the Lifshitz-Slyozov-Wagner equation as follows [24]:

$$d^3=\frac{64C_\infty\sigma\Omega^2t}{9RT}D_0\exp(-\frac{Q}{RT}) \quad (4)$$

The logarithm of both sides obtains the following equation:

$$\ln(d^3/t)=\ln(\frac{64C_\infty\sigma\Omega^2}{9RT}D_0)-\frac{Q}{RT} \quad (5)$$

where d is the average grain diameter, C_∞ is the molar solid solubility of diffusion elements, σ is the interfacial energy, Ω is the molar volume, and D_0 is the pre-exponential factor.

Figure 9(c) displays the fitting result on the growth behavior of grain in Zone II. The growth activation energy of α_2 phase is fitted to be 253 kJ/mol, which is lower than that of β/*B*2 phase in Zone I. It means that the formation of α_2 phase in the joint is easier than β/*B*2 phase, which can be ascribed to faster diffusion of Al element into the joint due to smaller atom size. It has been reported that Al element can strongly stabilize α_2 phase [25]. Therefore, the formation of α_2 phase is more preferential than β/*B*2 phase in the joint. In Zone III, when the bonding temperature was 900 °C, the

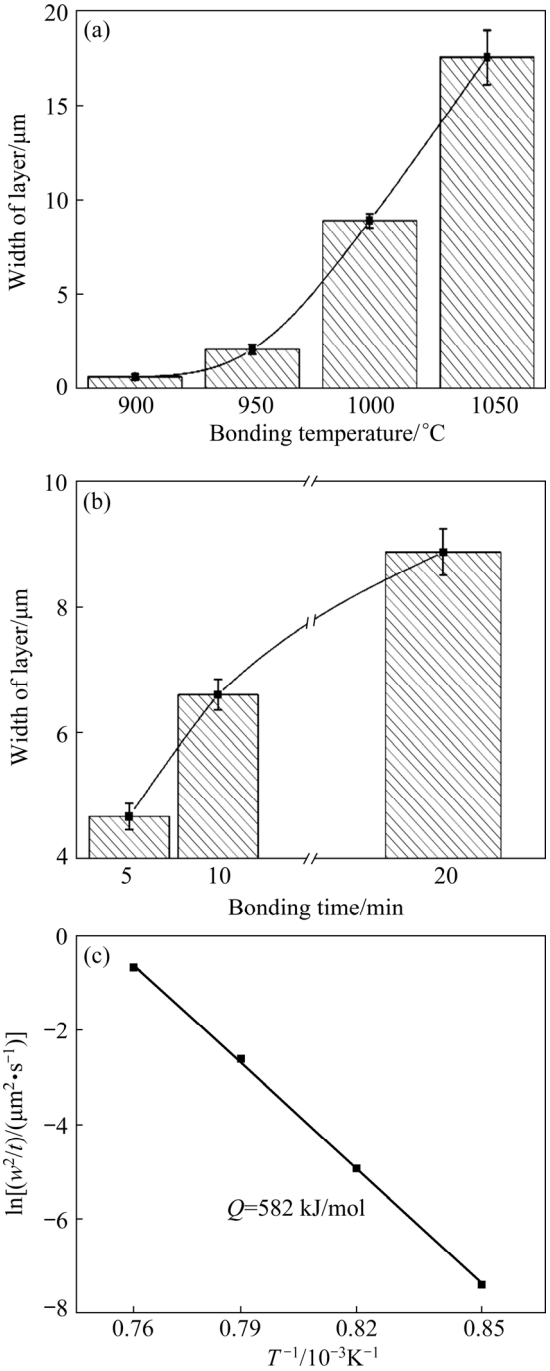

Fig. 7 Width of diffusion Zone I under different parameters: (a) Different bonding temperatures at 10 MPa and 10 min; (b) Different time at 1000 °C and 10 MPa; (c) Growth activation energy of β/*B*2 phase in Zone I

α-Ti nearly occupied all the Zone III. When the bonding temperature rose to 950 °C, light gray lamellar β-Ti can be obviously detected, as displayed in Fig. 3(a). With bonding temperature further increasing, the fraction of β-Ti increased due to more Nb, Cr and Mn atoms diffusing into Ti interlayer because of enhanced diffusion ability, as

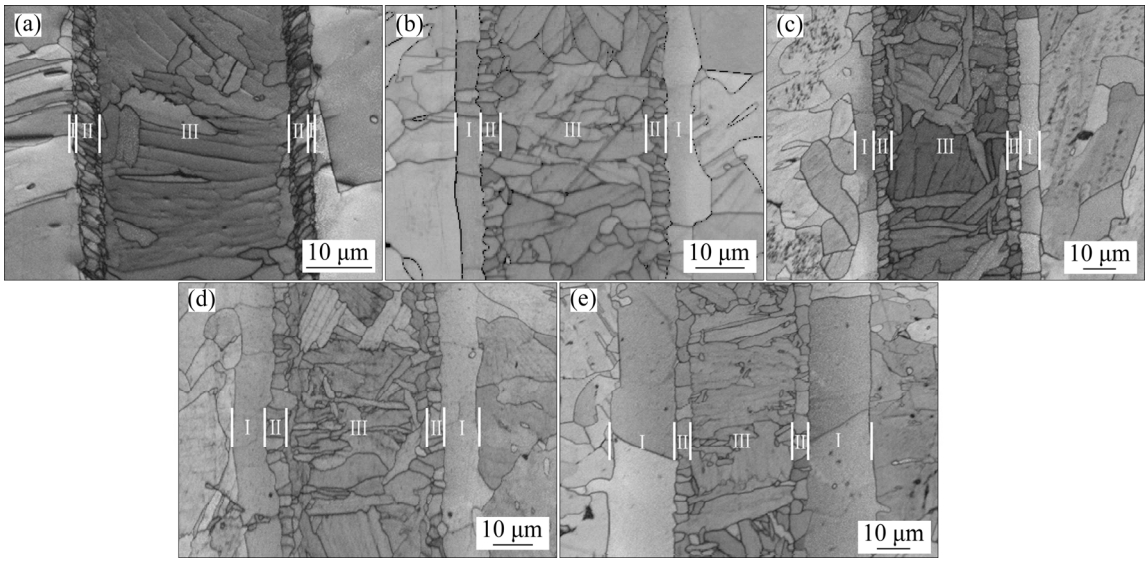

Fig. 8 Band contrast map of HNBG alloy joints bonded with Ti foil at 10 MPa: (a) 900 °C, 10 min; (b) 1000 °C, 5 min; (c) 1000 °C, 10 min; (d) 1000 °C, 20 min; (e) 1050 °C, 10 min

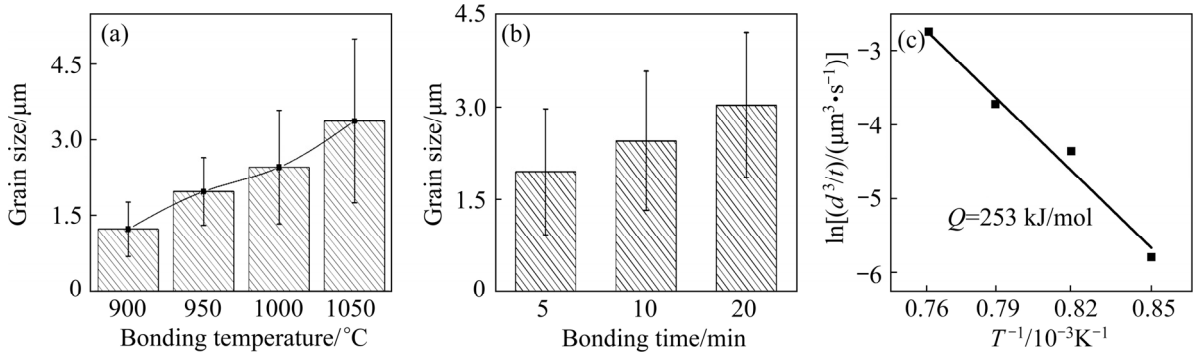

Fig. 9 Average grain size of α-Ti in Zone II under different parameters: (a) Different bonding temperatures at 10 MPa and 10 min; (b) Different time at 1000 °C and 10 MPa; (c) Growth activation energy of α_2 phase in Zone II

can be seen from Fig. 10(a). Figures 5(b)−(d) display the interfacial microstructure at 1000 °C for different time. The diffusion fluxes of Al, Nb, Mn and Cr from HNBG alloy towards Ti and inverse diffusion flux of Ti still existed when the bonding time was 20 min, as shown in Fig. 5(f). Therefore, with the bonding time extending from 5 to 20 min, Al, Nb, Mn and Cr atoms continuously diffused into Ti interlayer and Ti atoms also continuously diffused into HNBG alloy driven by concentration gradient. As a result, the width of Zone I (see Fig. 7(b)) increased by the bonding time, and relationship of both presents the convex parabola. The average grain size of α_2 in Zone II (see Fig. 9(b)) and the content of β-Ti in Zone III (see Fig. 10(b)) also increased when the bonding time extended.

From the above joint microstructure analysis, it can be concluded that the thickness of $\beta/B2$ phase layer in Zone I, the grain size of α_2 phase in Zone II and the content of β-Ti phase in Zone III increase with the increase of bonding temperature or bonding time. The $B2$ and α_2 phases are brittle phases, which are generally considered as detriment to the joint strength. However, the brittle phases are impossible to be completely delaminated in the joining of TiAl alloy. Luckily, it has been found that the brittle phase benefits the increase of joint strength with the thickness lower than the critical value; however, the mechanical properties of joints will be reduced with the thickness of brittle phase exceeding the critical value [23]. In addition, it has been reported that the shear strength increased with the growth of dynamic recrystallization grains in the joint [26]. Moreover, the increase of β-Ti phase reduces the plastic deformation ability of interlayer,

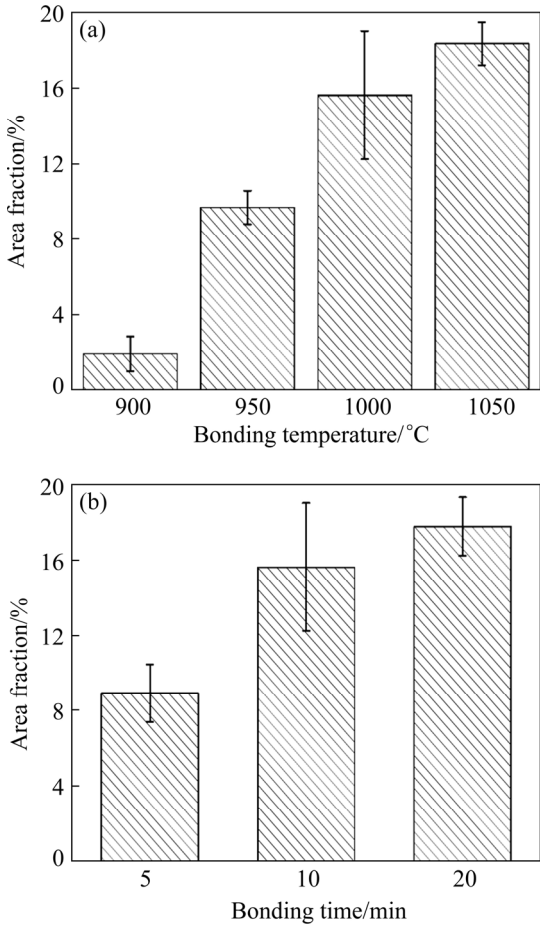

Fig. 10 Area fraction of β-Ti in Zone III at 10 MPa: (a) Different bonding temperatures for 10 min; (b) Different time at 1000 °C

which leads to weakening the function of relieving residual stress of joint. Therefore, there must exist the optimum combination of the thickness of β/$B2$ phase layer, the average grain size of α_2 phase and the content of β-Ti phase in the joint, which corresponds to the maximal shear strength.

3.3 Joint mechanical properties and fracture analysis of HNBG alloy bonded with Ti foil

Figure 11 displays the Vicker's microhardness across the HNBG alloy joint bonded at 1000 °C, 10 MPa and 10 min. It can be observed that the hardness value in the Zone I is higher than that in the Zone III. This can be ascribed to the formation of $B2$ phase in the Zone I which is more brittle than β-Ti phase due to the ordering transformation of β to $B2$. It is generally accepted that there is positive correlation between hardness and brittleness [27]. Therefore, the hardness of $B2$ phase is higher than that of β-Ti phase. In addition, the β-Ti phase is harder than α-Ti phase in Ti alloys [28]. As a result, the Zone I with $B2$ phase has a high hardness. The hardness of HNBG alloy substrate is lower than that in the Zone I due to the γ phase being softer than $B2$ phase [29].

Figure 12 shows shear strength of HNBG alloy joints bonded under different conditions. It can be observed that the shear strength first rose and then decreased with increasing the bonding

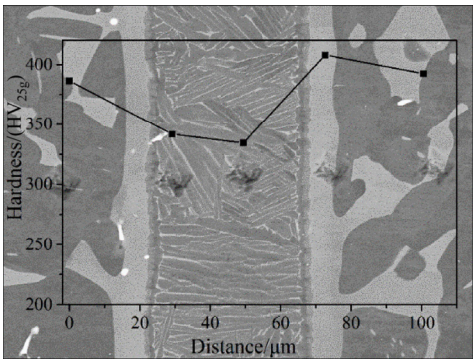

Fig. 11 Microhardness distribution in HNBG alloy joint bonded with Ti foil at 1000 °C, 10 MPa and 10 min

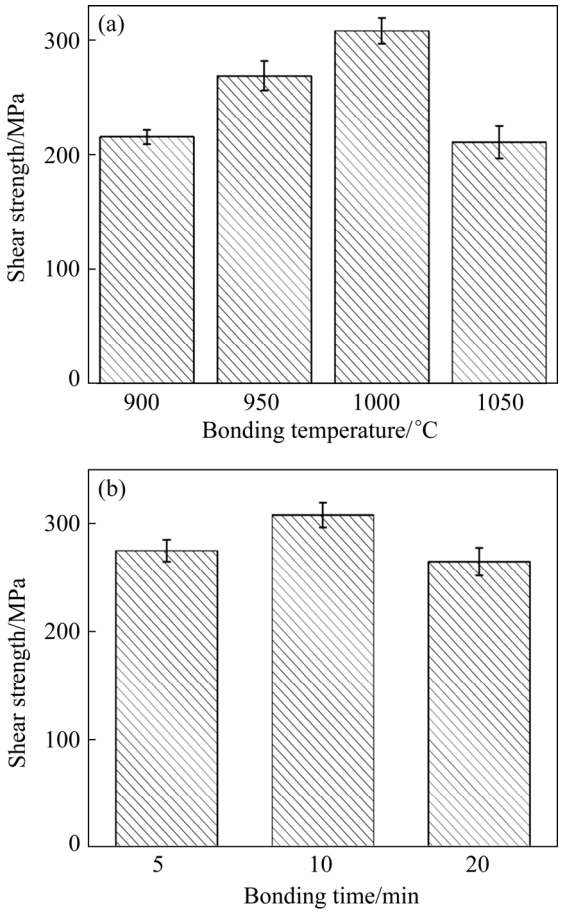

Fig. 12 Shear strength of HNBG alloy joints bonded with Ti foil at 10 MPa: (a) Different bonding temperatures for 10 min; (b) Different time at 1000 °C

temperature (see Fig. 12(a)). When the bonding temperature was 1000 °C, the maximum shear strength was 308 MPa, which was higher than that of the joint of the direct diffusion bonding of HNBG alloy at the same temperature [19]. The effect of bonding time on the joint shear strength is displayed in Fig. 12(b). It can be seen that the shear strength increased when the bonding time increased from 5 to 10 min while declining with the bonding time extending from 10 to 20 min. That is to say, the maximum shear strength was acquired at 1000 °C, 10 MPa and 10 min, which corresponds to the optimum bonding parameter. The thickness of $\beta/B2$ phase in the Zone I, the grain size of α_2 phase in the Zone II and the content of β-Ti phase in the Zone III achieved the optimal combination in the joint.

Figure 13 shows the fracture path of HNBG alloy joints bonded under different parameters. It can be observed that the propagation of crack mainly occurred along two different paths which were the interfaces between the Zone I and HNBG alloy, and between the Zone I and Zone II, respectively. However, when the bonding temperature reached 1000 °C, small part of cracks started to propagate into base alloys with bonding

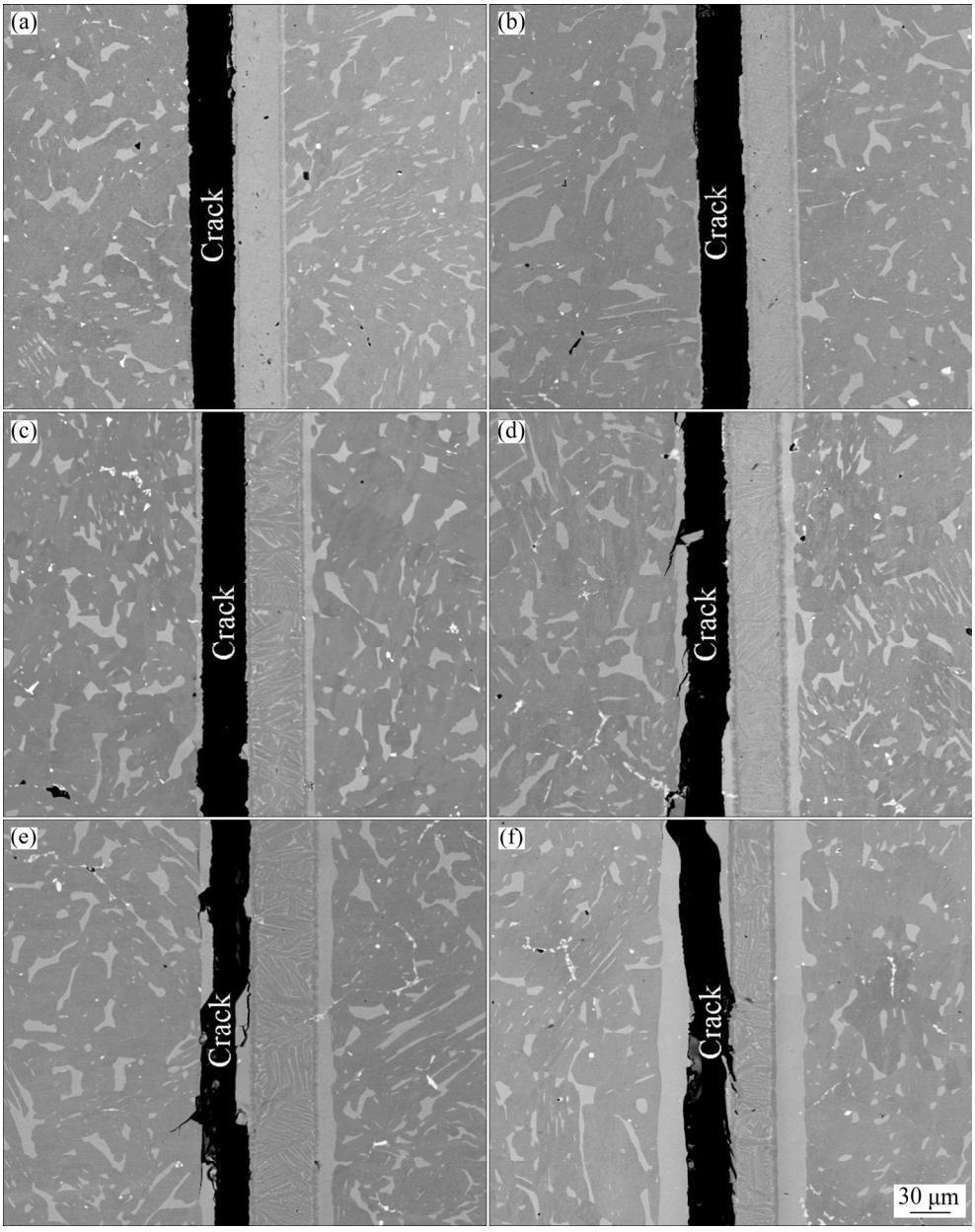

Fig. 13 Fracture paths of HNBG alloy joints bonded with Ti foil under different parameters: (a) 900 °C, 10 min, 10 MPa; (b) 950 °C, 10 min, 10 MPa; (c) 1000 °C, 5 min, 10 MPa; (d) 1000 °C, 10 min, 10 MPa; (e) 1000 °C, 20 min, 10 MPa; (f) 1050 °C, 10 min, 10 MPa

time of 10 and 20 min (see Figs. 13(d, e)). With the bonding temperature at 1050 °C, part of the cracks conversely tended to propagate to the Zone III (see Fig. 13(f)). Therefore, it can be concluded that Zone I was the weak area of the joint, which was due to large residual stress caused by the more brittleness of *B*2 phase compared with other phases in the joint.

Figure 14 shows fracture morphology of HNBG alloy joint bonded at 1000 °C, 10 MPa and 10 min. It can be seen that fracture surface is approximately divided into two parts (see Figs. 14(a) and (b)). From the local magnified pictures of Figs. 14(a) and (b), it can be observed that the fracture morphology is characterized by notch on Ti foil side (see Fig. 14(c)) or corresponding bulges on the HNBG alloy side(see Fig. 14(e)) due to curved interface between the Zone I and Zone II and flat area (see Figs. 14(d) and (f)) on both sides because of straight interface between the Zone I and HNBG alloy. Therefore, the fracture mode in HNBG alloy joints was brittle fracture along the phase boundary. The XRD analysis was additionally conducted on the fracture surface, as can be seen from Fig. 15. On the HNBG alloy side, the peaks of the γ and *B*2 phases were observed, while those of *B*2 and α_2 phases were observed on the Ti foil side, corroborating the above analysis on the fracture path of the HNBG alloy joint bonding with Ti foil.

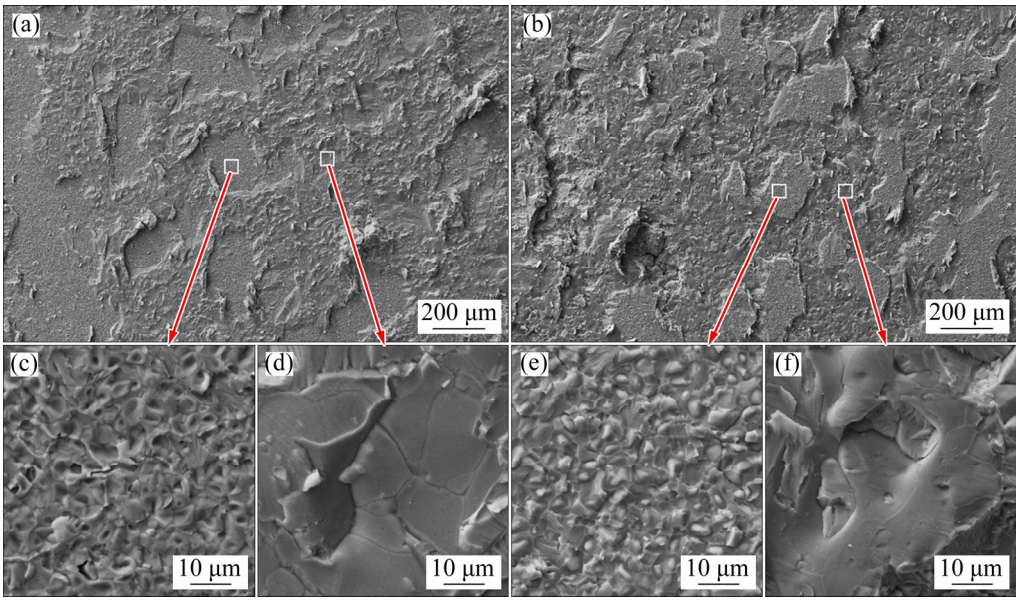

Fig. 14 Fracture morphologies of HNBG alloy joints bonded with Ti foil at 1000 °C, 10 MPa and 10 min: (a) Ti foil side; (b) HNBG alloy side; (c, d) Local amplification of (a); (e, f) Local amplification of (b)

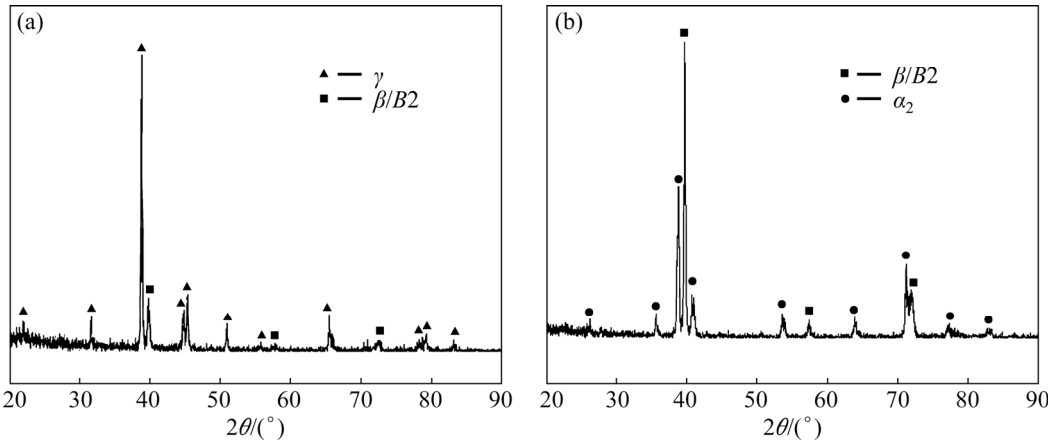

Fig. 15 XRD patterns of fracture surface of HNBG alloy joints bonded with Ti foil at 1000 °C, 10 MPa and 10 min: (a) HNBG alloy side; (b) Ti foil side

4 Conclusions

(1) The interface of the HNBG alloy bonding with Ti foil consisted of three diffusion zones. The $\beta/B2$ phase formed in the diffusion Zone I, α_2 phase in the diffusion Zone II, and β-Ti and α-Ti phases in the diffusion Zone III. The orientation relationship of the interface between $\beta/B2$ phase in the diffusion Zone I and γ phase in the HNBG alloy follows $\{111\}_{\gamma}//\{110\}_{\beta/B2}$, $\langle 110\rangle_{\gamma}//\langle 111\rangle_{\beta/B2}$.

(2) The thickness of $\beta/B2$ phase in the diffusion Zone I, the average grain size of α_2 phase in the diffusion Zone II and the amount of β phase in the diffusion Zone III increased with the increase of bonding temperature or bonding time. The growth activation energies of $\beta/B2$ and α_2 phase are 582 and 253 kJ/mol, respectively. The formation of α_2 phase is easier than $\beta/B2$ phase in the joint.

(3) The maximum shear strength of the joint was 308 MPa at 1000 °C, 10 MPa and 10 min, at which the optimum combination of the thickness of $\beta/B2$ phase, the average grain size of α_2 phase and the content of β phase was obtained in the joint.

(4) Fracture mainly occurred along the interfaces between the Zone I and HNBG alloy and between the Zone I and Zone II. As the bonding temperature reached 1000 °C, part of cracks propagated into base alloys. However, part of the cracks conversely tended to propagate to Zone Ⅲ at bonding temperature 1050 °C. Zone I was the weak area of the HNBG alloy joint. The fracture mode showed brittleness rupture along the phase boundary.

Acknowledgments

This work was supported by the National Natural Science Foundation of China (Nos. 51871012, 52071021), Beijing Natural Science Foundation (No. 2162024), Fundamental Research Funds for the Central Universities, China (No. FRF-GF-20-20B), and the National Key Basic Research Program of China (No. 2011CB605502).

References

[1] QIU Cong-zhang, LIU Yong, HUANG Lan, LIU Bin, ZHANG Wei, HE Yue-hui, HUANG Bai-yun. Tuning mechanical properties for $\beta(B2)$-containing TiAl intermetallics [J]. Transactions of Nonferrous Metals Society of China, 2012, 22: 2593−2603.

[2] GE Geng-wu, ZHANG Lai-qi, XIN Jin-jin, LIN Jun-pin, AINDOW M, ZHANG Li-chun. Constitutive modeling of high temperature flow behavior in a Ti−45Al−8Nb−2Cr−2Mn−0.2Y alloy [J]. Scientific Reports, 2018, 8: 5453.

[3] ZHANG Yu, WANG Xiao-peng, KONG Fan-tao, SUN Liang-liang, CHEN Yu-yong. Microstructure, texture and mechanical properties of Ti−43Al−9V−0.2Y alloy hot-rolled at various temperatures [J]. Journal of Alloys and Compounds, 2019, 777: 795−805.

[4] TETSUI T, SHINDO K, KOBAYASHI S, TAKEYAMA M. A newly developed hot worked TiAl alloy for blades and structural components [J]. Scripta Materialia, 2002, 47: 399−403.

[5] LUO Y Y, XI Z P, ZENG W D, MAO X N, YANG Y L, NIU H Z. Characteristics of high-temperature deformation behavior of Ti−45Al−2Cr−3Ta−0.5W alloy [J]. Journal of Materials Engineering and Performance, 2014, 23: 3577−3585.

[6] ZHANG Lai-qi, GE Geng-wu, LIN Jun-pin, AINDOW M, ZHANG Li-chun. Effect of transition metal alloying elements on the deformation of Ti−44Al−8Nb−0.2B−0.2Y alloys [J]. Scientific Reports, 2018, 8: 14242.

[7] CAM G, CLEMENS H, GERLING R, KOCAK M. Diffusion bonding of γ-TiAl sheets [J]. Intermetallics, 1999, 7: 1025−1031.

[8] LIN Peng, XI Xian-zheng, ZHAO Wen-kai, YANG Rui-hong, LIN Fei, CUI Xiao-lei, LIU Gang. Microstructure and mechanical properties of Ti−6Al−4V/Ti−22Al−25Nb joint formed by diffusion bonding [J]. Transactions of Nonferrous Metals Society of China, 2021, 31: 1339−1349.

[9] FENG Guang-jie, WEI Yan, HU Bing-xu, WANG Yi-feng, DENG De-an, YANG Xiu-xia. Vacuum diffusion bonding of Ti_2AlNb alloy and TC4 alloy [J]. Transactions of Nonferrous Metals Society of China, 2021, 31: 2677−2686.

[10] HERRMANN D, APPEL F. Diffusion bonding of γ(TiAl) alloys: Influence of composition, microstructure, and mechanical properties [J]. Metallurgical and Materials Transactions A, 2009, 40: 1881−1902.

[11] YAN P, WALLACH E R. Diffusion-bonding of TiAl [J]. Intermetallics, 1993, 1: 83−97.

[12] MASAHASHI N, HANADA S J, MIZUHARA Y J. Diffusion bonding associated with phase transformation in (γ+β) micro-duplex titanium aluminides [J]. Materials Transactions, 2001, 42: 1028−1034.

[13] DUARTE L I, RAMOS A S, VIEIRA M F, VIANA F, VIEIRA M T, KOÇAK M. Solid-state diffusion bonding of gamma- TiAl alloys using Ti/Al thin films as interlayers [J]. Intermetallics, 2006, 14: 1151−1156.

[14] WANG Y, WU X F, YANG Z W, XIA Y H, WANG D P. Microstructure and mechanical properties of Ti_3SiC_2/Ti_3SiC_2 diffusion bonded joints using Ti foil as an interlayer [J]. Ceramics International, 2019, 45: 20900−20909.

[15] TATARKO P, GRASSO S, SAUNDERS T G, CASALEGNO V, FERRARIS M, REECE M J. Flash joining of CVD-SiC coated C_f/SiC composites with a Ti interlayer [J]. Journal of the European Ceramic Society, 2017, 37: 3841−3848.

[16] LI Xiao, WANG Guo-feng, GU Yi-bin, YANG Jian-lei. Electrically assisted diffusion bonding of Ti_2AlNb alloy sheet using CP-Ti foil interlayer: Microstructural characterization

and mechanical tests [J]. Materials Science and Engineering A, 2019, 744: 733−745.
[17] MUNIR Z A, ANSELMI-TAMBURINI U A, OHYANAGI M. The effect of electric field and pressure on the synthesis and consolidation of materials: A review of the spark plasma sintering method [J]. Journal of Materials Science, 2006, 41: 763−777.
[18] ZHAO Kun, LIU Yong, HUANG Lan, LIU Bin, HE Yue-hui. Diffusion bonding of Ti−45Al−7Nb−0.3W alloy by spark plasma sintering [J]. Journal of Materials Processing Technology, 2016, 230: 272−279.
[19] GAO Qiang, WANG Ze-ming, ZHANG Lai-qi, GE Geng-wu. Joining of *β*-*γ* TiAl alloys containing high content of niobium by pulse current diffusion bonding [J]. Intermetallics, 2021, 133: 107184.
[20] ZHANG Bo-xian, CHEN Chun-huan, HE Jian-chao, HOU Jin-bao, CHAI Lu, LV Yan-long. Spark plasma diffusion bonding of TiAl/Ti_2AlNb with Ti as interlayer [J]. Materials, 2020, 13: E3300.
[21] ZHU Lei, TANG Bin, DING Ming-xuan, LIU Yan, CHEN Xiao-fei, YAN Shao-peng, LI Jin-shan. Interface characteristic and mechanical performance of TiAl/Ti_2AlNb diffusion bonding joint with pure Ti interlayer [J]. Rare Metals, 2020, 39: 1402−1412.
[22] LI Lin, LIU Li-bin, ZHANG Li-gang, ZENG Li-jun, ZHAO Yun, BAI Wei-min, JIANG Yu-rong. Phase equilibria of the Ti−Al−Nb system at 1000, 1100 and 1150 °C [J]. Journal of Phase Equilibria and Diffusion, 2018, 39: 549−561.
[23] LI Peng, WANG Shuai, XIA Yue-qing, HAO Xiao-hu, DONG Hong-gang. Diffusion bonding of $AlCoCrFeNi_{2.1}$ eutectic high entropy alloy to TiAl alloy [J]. Journal of Materials Science & Technology, 2020, 45: 59−69.
[24] LAPIN J, VAŇO A. Coarsening kinetics of *α*- and *γ*′-precipitates in a multiphase intermetallic Ni–Al–Cr–Ti type alloy with additions of Mo and Zr [J]. Scripta Materialia, 2004, 50: 571−575.
[25] SUN Wei, YOU Feng-hai, KONG Fan-tao, WANG Xiao-peng, CHEN Yu-yong. Fracture mechanism of a high tensile strength and fracture toughness Ti6Al4V−TiAl laminated composite [J]. Journal of Alloys and Compounds, 2020, 820: 153088.
[26] ÇAM G, MÜLLAUER J, KOÇAK M. Diffusion bonding of two phase *γ*-TiAl alloys with duplex microstructure [J]. Science and Technology of Welding and Joining, 1997, 2: 213−219.
[27] SUN Wei, YANG Fei, KONG Fan-tao, WANG Xiao-peng, CHEN Yu-yong. Interface characteristics of Ti6Al4V−TiAl metal-intermetallic laminate (MIL) composites prepared by a novel hot-pack rolling [J]. Materials Characterization, 2018, 144: 173−181.
[28] WANG Y, CAI X Q, YANG Z W, WANG D P, LIU X G, LIU Y C. Diffusion bonding of Ti2AlNb alloy using pure Ti foil as an interlayer [J]. Journal of Alloys and Compounds, 2018, 756: 163−174.
[29] KLIMOVÁ A, LAPIN J. The effect of heat treatment on microstructure and hardness of in-situ Ti−38Al−7.5Nb−5C−0.9Mo composite [J]. Kovove Materialy, 2020, 58: 433−443.

高铌 *β*−*γ* TiAl 合金加 Ti 箔中间层的等离子烧结扩散连接行为

高 强，张来启，乔 祎，林均品

北京科技大学 新金属材料国家重点实验室，北京 100083

摘 要：采用放电等离子烧结技术，以纯钛为中间层，对高铌 *β*−*γ* TiAl 合金(HNBG)进行扩散连接，对接头的显微组织演变、生长动力学和力学性能进行研究。接头包括三个扩散区，分别是 I 区形成 *β*/*B*2 相，II 区形成 α_2 相，III 区形成 *β*-Ti 相和 *α*-Ti 相。*β*/*B*2 相的厚度、α_2 相的平均晶粒尺寸和 *β*-Ti 相的含量随着连接温度或时间的增加而增加。*β*/*B*2 相和 α_2 相的生长活化能分别为 582 和 253 kJ/mol。在 1000 ℃，10 min，10 MPa 下接头达到最大剪切强度 308 MPa。断裂主要发生在扩散区 I 和 HNBG 合金之间以及扩散区 I 和扩散区 II 之间的界面上。HNBG 合金接头的断裂机制为沿着相界的脆性断裂。

关键词：高铌 *β*−*γ* TiAl 合金；扩散连接；放电等离子烧结；中间层；显微组织演化；力学性能

(Edited by Xiang-qun LI)